A New Function Expansion for Polarization Coherence Tomography

Hong Zhang, *Member, IEEE*, Peifeng Ma, and Chao Wang, *Member, IEEE*

***Abstract*—In this letter, we investigate the polarization coherence tomography technique and propose a new function expansion to reconstruct the vertical profile function. Instead of generating profile in Fourier–Legendre series, we deduce orthogonal functions on $[-1, 1]$ by weight of z^2, which can increase the highest polynomial order and decrease the condition number of the inversion matrix, indicating that the inversion in the new expansion is more stable and less susceptible to noise. Finally, we apply the technique to simulated dual-baseline data and Chinese X-band single-baseline polarimetric synthetic aperture radar interferometry data to demonstrate its validity and robustness.**

***Index Terms*—Function expansion, polarization coherence tomography (PCT), vertical profile function.**

I. Introduction

POLARIMETRIC synthetic aperture radar (SAR) interferometry (POLinSAR) [1] is a new branch of radar interferometry which combines radar polarimetry and interferometry: it allows locating scattering mechanisms as functions of height. It has been proved that the known applications of POLinSAR are forest height and biomass as well as emerging applications in agriculture. New 3-D techniques have been developed along with the multibaseline interferometric measurements. One of the simplest new 3-D methods is polarization coherence tomography (PCT) proposed by Cloude in 2006 [2]. Assuming that vegetation height and underlying surface topography have been obtained, after normalizing the range of the integral of the volume scattering complex coherence formulation, profile coefficients of a specific polarization channel can be estimated by constructing identity relations between complex coherence and expansion function in Fourier–Legendre (F–L) orthogonal polynomials. Then, the vertical profile function can be represented by the coefficients and F–L polynomials. Cloude [2] has shown that, even for one baseline, the general shape of single-layered volume can be calculated.

Tomography reduces to a solution of a set of linear equations for the unknown coefficients using PCT technology. As for single-baseline data, only two unknown coefficients can be obtained in F–L series; that is to say, the highest order of polynomials is two, which limits the approximation resolution. In order to achieve higher accuracy of the estimation, we must employ multibaseline data, however, which is expensive and difficult to obtain. While dual-baseline data can be used to introduce another two F–L polynomials, their poor condition that defines the stability of inversion and sensitivity to noise confines the application. Therefore, whether we can reduce the condition number (CN) of the inversion matrix is critical to the final results and according to the dual-baseline scenario in [3], a regularization technique has been proposed at the cost of loss of precision. In addition, F–L polynomials are orthogonal on $[-1, 1]$ by weight of one. In practice, for various-two-layer-model mixed-surface-plus-volume cases, nevertheless, scattering amplitude is stronger on the top of canopy, corresponding to volume scattering, and near the ground, corresponding to surface–canopy dihedral response. For the several reasons above, we investigate the feasibility of reconstructing the vertical profile function in a new orthogonal family in this letter.

This letter is organized as follows. We first review the PCT method proposed by Cloude [2]–[4] in Section II. Then, the PCT with a new function expansion is proposed in Section III. In Section IV, the validity of this expansion is demonstrated using simulated data; furthermore, we evaluate the stability of this approximation approach and compare it with the results in the F–L series by Cloude in simulated and real scenarios. Finally, some conclusions are given in Section V.

II. PCT in F–L Series

The main observable in PCT is the complex interferometric coherence

$$\widetilde{\gamma} = e^{ik_z z_0} \frac{\int\limits_0^{h_v} f(z) e^{ik_z z}\, dz}{\int\limits_0^{h_v} f(z)\, dz} = e^{i\varphi_0} \frac{\int\limits_0^{h_v} f(z) e^{ik_z z}\, dz}{\int\limits_0^{h_v} f(z)\, dz} \quad (1)$$

where z_0 is the position of the bottom of the scattering layer, φ_0 is the topographic phase, and $f(z)$ is the vertical structure function.

This coherence depends on vertical structure variations in the scene due, for example, to the presence of vegetation cover [1]–[3], and we can use this dependence to devise a method for 3-D imaging. To demonstrate this, Cloude defined a vertical structure function $f(z)$, which represents the vertical variation of microwave scattering at a point in the 2-D radar image. The reconstruction of the function $f(z)$ from $\widetilde{\gamma}$ at each point in the image is then termed coherence tomography. To proceed,

Manuscript received April 24, 2011; revised August 22, 2011 and October 28, 2011; accepted December 14, 2011. Date of publication March 2, 2012; date of current version May 29, 2012. This work was supported in part by the National Natural Science Foundation of China under Grant 40971198 and in part by the 863 Program under Grant 2009AA12Z118.

The authors are with the Key Laboratory of Digital Earth, Center for Earth Observation and Digital Earth, Chinese Academy of Sciences, Beijing 100094, China (e-mail: hzhang@ceode.ac.cn; cwang@ceode.ac.cn).

Color versions of one or more of the figures in this paper are available online at http://ieeexplore.ieee.org.

Digital Object Identifier 10.1109/LGRS.2012.2183113

assuming that the function $f(z)$ is bounded (by the underlying surface and top of the vegetation layer, for example) and so can be expanded efficiently in terms of a set of simpler functions, the F–L series is shown in

$$f(z')=\sum_n a_n P_n(z'), \qquad a_n=\frac{2n+1}{2}\int_{-1}^{1} f(z')P_n(z')\,dz' \quad (2)$$

where $P(z)$ represents the standard Legendre polynomials, with

$$P_0(z)=1 \qquad P_1(z)=z \qquad P_2(z)=\frac{1}{2}(3z^2-1)$$
$$P_3(z)=\frac{1}{2}(5z^3-3z) \qquad P_4(z)=\frac{1}{8}(35z^4-30z^2+3). \quad (3)$$

It is shown that increasing the number of baselines leads to more terms in the series and, hence, to a higher resolution.

The reconstruction of coherence tomography is inevitably subject to the effect of noise, such as temporal decorrelation, statistical fluctuations in coherence estimation, and coherence bias with limited data samples. Therefore, the sensitivity to noise is a key point that we should consider. In 2007, Cloude improved the solution method by filtering the singular matrix in the dual-baseline case [3] to obtain the stability by reducing the precision of estimation.

III. PCT Using New Function Expansion

It can be noted in Cloude's method [3] that the strong scattering of the forest lies in the canopy and ground surface, corresponding to volume scattering and ground–trunk dihedral scattering mechanisms, respectively. In order to increase the weights of the canopy and the ground–trunk scattering, after converting the transformation range of the vertical height from $[0, h_v]$ to $[-1, 1]$, we introduce the orthogonal series by weight of z^2 for expansion, where z represents the vertical position. Therefore, compared with F–L expansion by weight of one, the simulated scattering profile structure in the new expansion is more in line with physical mechanism.

In our method, the first few polynomials $P'(z)$ are shown as

$$P'_0(z)=1 \qquad P'_1(z)=z \qquad P'_2(z)=\frac{1}{2}(5z^2-3)$$
$$P'_3(z)=\frac{1}{2}(7z^3-5z) \qquad P'_4(z)=\frac{1}{8}(63z^4-70z^2+15). \quad (4)$$

To retrieve the vertical structure $f(z)$ in the functions in (4), we first normalize the range of the integral by a change of variable $z'=(2z/h_v)-1$; the results are shown in

$$\int_0^{h_v} f(z)e^{ik_z z}\,dz=\frac{h_v}{2}e^{i\frac{k_z h_v}{2}}\int_{-1}^{1} g(z')e^{i\frac{k_z h_v}{2}z'}\,dz'$$
$$\int_0^{h_v} f(z)\,dz=\frac{h_v}{2}\int_{-1}^{1} g(z')\,dz'. \quad (5)$$

Instead of expanding the function $g(z')$ directly into Legendre polynomials [2], [3], we assume that $g(z')=q(z')z'^2$.

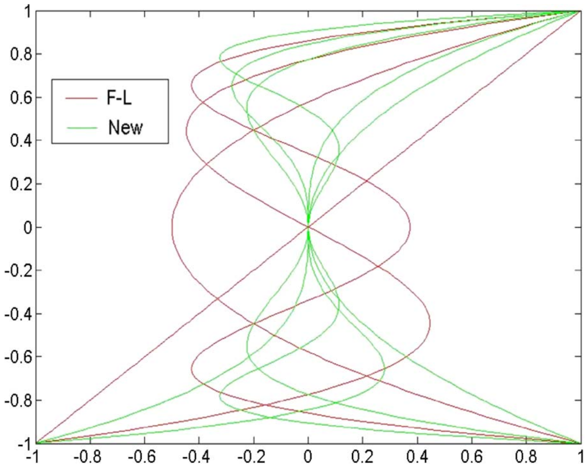

Fig. 1. Plot of basis functions of two expansions.

Since the function $g(z')$ to be reconstructed is nonnegative, the function $q(z')$ is also nonnegative, and then, we rescale the range $q(z')=1+a(z')$ so that $a(z')\geq -1$. Now, we can replace the function $a(z')$ with the orthogonal series on $[-1, 1]$ as $a(z')=\sum_n a_n P'_n(z')$. Then, the real polynomials used to approximate can be written as $Q_n(z)=z^2 P'_n(z)$, and

$$\int_{-1}^{1} P_n^2(z)\,dz > \int_{-1}^{1} Q_n^2(z)\,dz. \quad (6)$$

That is, the squared integral of our new function is less than that of the Legendre function. Fig. 1 shows the comparison of basis functions between two expansions, and we can see that our new function is more compact in the vertical direction. We can conclude that the same variation of the profile coefficient is less affected on the profile function expanded by our method, i.e., the new expansion method has lower sensitivity.

By expanding series and collecting terms, $\widetilde{\gamma}$ can be simplified as

$$\begin{aligned}\widetilde{\gamma}^{-i\varphi_0}e^{-ik_v} &= \widetilde{\gamma}_k = \frac{\int_{-1}^{1}\left(1+a_0P'_0(z')+a_1P'_1(z')+\cdots\right)z'^2 e^{ik_v z'}\,dz'}{\int_{-1}^{1}\left(1+a_0P'_0(z')\right)z'^2 e^{ik_v z'}\,dz'}\\ &= \frac{(1+a_0)f_0+a_1f_1+a_2f_2+\cdots+a_nf_n}{(1+a_0)}\\ &= f_0+a_{10}f_1+a_{20}f_2+\cdots+a_{n0}f_n \end{aligned} \quad (7)$$

where $k_v=h_v k_z/2$. Note that the denominator value is simplified for orthogonality of high-order polynomials so that it becomes a constant. Then, we can normalize the unknown coefficients by a zero-order term

$$a_{n0}=\frac{a_n}{1+a_0}. \quad (8)$$

The evaluation of each component involves the determination of the function f_i; we give explicit forms of these functions up to four orders in

$$\begin{aligned} f_0 &= \left(\frac{3}{k_v} - \frac{6}{k_v^3}\right)\sin(k_v) + \frac{6\cos(k_v)}{k_v^2} \\ f_1 &= i\left(\left(\frac{18}{k_v^3} - \frac{3}{k_v}\right)\cos(k_v) + \left(\frac{9}{k_v^2} - \frac{18}{k_v^4}\right)\sin(k_v)\right) \\ f_2 &= \left(\frac{21}{k_v^3} - \frac{180}{k_v^4}\right)\cos(k_v) + \left(\frac{3}{k_v} - \frac{81}{k_v^3} + \frac{180}{k_v^5}\right)\sin(k_v) \\ f_3 &= i\left(\left(\frac{165}{k_v^3} - \frac{1260}{k_v^5} - \frac{3}{k_v}\right)\cos(k_v)\right. \\ &\qquad \left. + \left(\frac{9}{k_v^2} - \frac{585}{k_v^4} + \frac{1260}{k_v^6}\right)\sin(k_v)\right) \\ f_4 &= \left(-\frac{2205}{k_v^4} + \frac{17\,010}{k_v^6} + \frac{48}{k_v^2}\right)\cos(k_v) \\ &\quad + \left(\frac{3}{k_v} - \frac{405}{k_v^3} + \frac{7875}{k_v^5} - \frac{17\,010}{k_v^7}\right)\sin(k_v). \end{aligned} \tag{9}$$

It can be noted as in the original PCT formulation [2] that the even index functions are real while odd functions are purely imaginary, and the functions vary only with the single parameter k_v.

If we can calculate the unknown coefficients a_{n0} by inverting this relation, the function of relative scattering density can be obtained as

$$\hat{g}(z') = z'^2(1 + a_{10}P_1'(z') + a_{20}P_2'(z') + \cdots + a_{n0}P_n'(z'), \quad -1 \le z' \le 1. \tag{10}$$

We can also change the variable range to the interval $[0, h_v]$; then, it is written as

$$f(z) = \left(\frac{2z}{h_v} - 1\right)^2 \left(1 + a_{10}P_1'\left(\frac{2z}{h_v} - 1\right) + \cdots + a_{n0}P_n'\left(\frac{2z}{h_v} - 1\right)\right), \quad 0 \le z \le h_v. \tag{11}$$

Before estimation of the unknown parameters a_{n0}, we must have *a priori* knowledge of topographic phase and vegetation height. Many efficient algorithms have been proposed to retrieve these two parameters using POLinSAR data, and in this letter, we employ a three-stage procedure [5]. Once we know the real evaluation of height and topographic phase, relative profile coefficients can be computed. As for single-baseline data, two coefficients a_{10} and a_{20} can be shown in

$$a_{10} = \mathrm{Im}(\widetilde{\gamma}_k)/f_1 \qquad a_{20} = (\mathrm{Re}(\widetilde{\gamma}_k) - f_0)/f_1. \tag{12}$$

That is to say, the first three polynomials can be used to approximate. As for dual-baseline data, another two higher order polynomials will be added to improve approximation resolution. Similarly, the linear formulation can be written as shown in

$$\begin{bmatrix} 1 & 0 & 0 & 0 & 0 \\ 0 & f_1^A & 0 & f_3^A & 0 \\ 0 & 0 & f_2^A & 0 & f_4^A \\ 0 & f_1^B & 0 & f_3^B & 0 \\ 0 & 0 & f_2^B & 0 & f_4^B \end{bmatrix} \begin{bmatrix} a_{00} \\ a_{10} \\ a_{20} \\ a_{30} \\ a_{40} \end{bmatrix} = \begin{bmatrix} 1 \\ \mathrm{Im}\left(\widetilde{\gamma}_k^A\right) \\ \mathrm{Re}\left(\widetilde{\gamma}_k^A\right) - f_0^A \\ \mathrm{Im}\left(\widetilde{\gamma}_k^B\right) \\ \mathrm{Re}\left(\widetilde{\gamma}_k^B\right) - f_0^B \end{bmatrix} \tag{13}$$

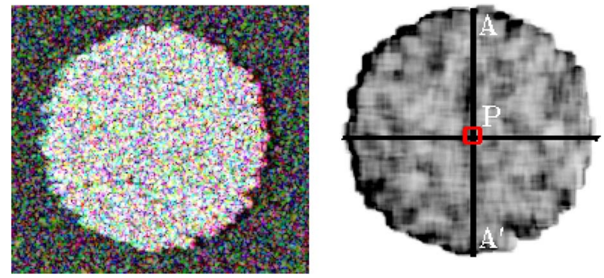

Fig. 2. (Left) L-band simulation of a 10-m vegetation layer above a rough surface. (Right) Coherence of HV polarization ($looks = 11$).

where superscripts A and B relate to the two baselines used and $a[]$ represents the profile coefficients. We can denote (13) as

$$[F]a = g \tag{14}$$

the solution can be obtained as $a = [F]^{-1}g$. From the vector $a[]$, the normalized vertical structure function can be estimated for a known layer depth k_v.

IV. Experimental Results

In order to demonstrate the effectiveness of the new function expansion in the generation of coherence tomography, we employ POLinSAR dual-baseline data simulated on the basis of two-layer models by European-Space-Agency-released POLSARPro. The SAR simulator is set using a 2-D point spread function with 1.5-m azimuth and 1.06 ground range resolution. The center frequency is 1.3 GHz (L-band) and at 45° angle of incidence from 3-km altitude. The first baseline is configured 10 m horizontal and 1 m vertical, while the second is 15 m horizontal and 5 m vertical. The forest is initialized deciduous with a height of 10 m. Fig. 2 shows the simulated Pauli decomposition image of the forest and the coherence of HV polarization.

We use the three-stage method to estimate the height map of the simulated POLinSAR forest data [5]. The estimated height ranges from 5 to 15 m with a mean of 9.02 m, which is close to the true height of 10 m. Then, we employ the estimated forest height and topography phase to develop the vertical structure. The vertical scattering function of one pixel P and the tomography along range line AA' in the HV polarization channel estimated by three methods, namely, F–L expansion [2], improved F–L expansion [3], and our method, are shown in Figs. 3 and 4.

Now, we evaluate the new method in terms of approximation precision and stability. Take the HV polarization channel, for example, in the dual-baseline system configuration; the simulated vertical scattering intensity function generally has two strong points. The first is the scattering center of the volume scattering mechanism, located in the canopy, not the highest point of the tree but a slightly lower part of the top. Because the simulated vegetation type is broad-leaved forest, the most dense leaves and branches are located not at the highest point but at a slightly lower part of the top. The second strong point is the ground–trunk dihedral scattering, which is slightly higher than the ground but not the lowest point of the tree. Moreover, in the HV polarization channel, the volume scattering is dominant; the intensity of the volume scattering is higher than the intensity of

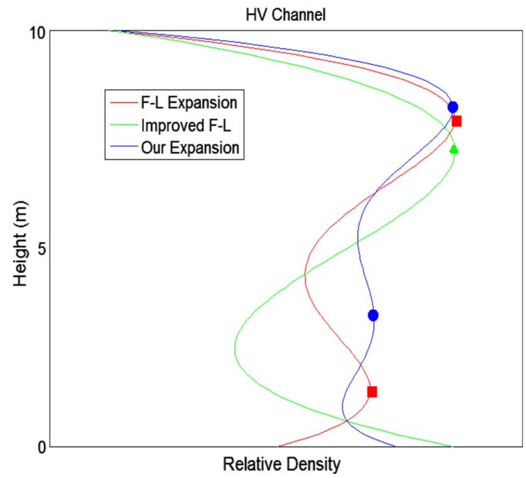

Fig. 3. Profiles of the HV polarization channel at point P in Fig. 2 estimated by three methods: F–L expansion [2], improved F–L expansion [3], and our method.

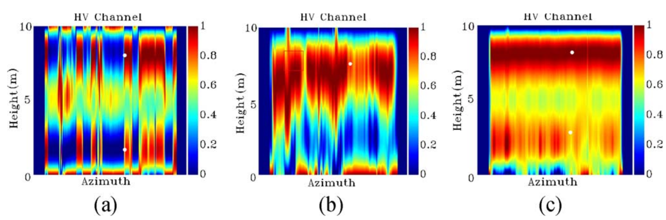

Fig. 4. Polarimetric tomographic reconstructions of the HV polarization channel along range line AA' in Fig. 2 estimated by three methods: (a) F–L expansion [2], (b) improved F–L expansion [3], and (c) our method. The white dots indicate the strongest points.

the ground–trunk dihedral scattering. From Fig. 3, we can see that both of the results estimated by the F–L method and our method have two strong points, shown as blue dots and red solid block, respectively, and the intensity of the volume scattering is higher than the intensity of the ground–trunk dihedral scattering. Fig. 4(a) and (c) also shows the same results. However, there is only one strong point corresponding to the volume scattering mechanism in the green curve in Figs. 3 and 4(b), similar to the result of the HV polarization channel in the single-baseline case. The reason for this is that the improved F–L method is to achieve high stability by reducing the simulation accuracy [3].

Next, we analyze the stability of the three methods. As the CN of the F–L expansion in the dual-baseline case is relatively large, the stability is not high; many points in Fig. 4(a) cannot be properly inversed because of the impact of coherence noise. The locations of the simulated scattering centers of a row of trees vary greatly, without continuity. In Fig. 4(b) and (c), the scattering centers of a row of trees are relatively stable. Moreover, comparing the variances of the profile coefficients of the three methods, shown in Table I, we can draw that the variances of the profile coefficients of our method are the minimum among the three methods; that is to say, it is the least sensitive to noise.

To substantiate our conclusion, we turn to mathematical demonstration. From the matrix inversion formula $[F]a = g$, we find that the stability of inversion is attributed to the CN of matrix $[F]$. In the single-baseline case, $CN = -(1/f_2)$; the detailed analysis was shown in the literature [2]. In terms of F–L expansion

TABLE I
STANDARD DEVIATIONS OF THE PROFILE COEFFICIENTS FOR THE HV POLARIZATION CHANNEL IN THE THREE METHODS

Parameters	F-L expansion	Improved F-L expansion	Our expansion
a_{10}	0.42	0.29	0.23
a_{20}	0.85	0.73	0.66
a_{30}	1.54	1.37	1.25
a_{40}	13.20	0.02	0.003

$$CN_{\mathrm{FL}-S} = -\frac{1}{f_2} = -\frac{k_v^2}{3\cos k_v - (3 - k_v^2)\frac{\sin k_v}{k_v}} \tag{15}$$

and in terms of our expansion, CN can be written as

$$CN_{\mathrm{New}-S} = -\frac{1}{3\frac{\sin k_v}{k_v} + 21\frac{\cos k_v}{k_v^2} - 81\frac{\sin k_v}{k_v^3} - 180\frac{\cos k_v}{k_v^4} + 180\frac{\sin k_v}{k_v^5}}. \tag{16}$$

In the dual-baseline case, matrices $[F]$ of the F–L expansion and the improved F–L expansion do not change [3]; we discuss the F–L expansion in the dual-baseline case in this letter. By defining the CN of matrix F, we can obtain

$$\begin{aligned} CN_D &= \|F\|_2 * \|F^{-1}\|_2 \\ &= \sqrt{\lambda_{\max}(F * F^{\mathrm{T}})} * \sqrt{\lambda_{\max}\left(F^{-1} * (F^{-1})^{\mathrm{T}}\right)} \end{aligned} \tag{17}$$

where F^{-1} is the inverse matrix of F, F^{T} is the transposed matrix of F, and $\lambda_{\max}$ is the maximum eigenvalue of F. Moreover, in the dual-baseline case, the F matrix changes with k_v; in general, we assume that the k_v value of the second baseline is unchanged.

Fig. 5 plots the two functions versus the normalized wavenumber in the singe- and dual-baseline cases. In our experiment, for dual-baseline tomography, we assume that the k_v value of the first baseline changes between [0, 1]; the k_v value of the second is one. We can see that, in both single- and dual-baseline cases, the values of CN in the approximation method of this letter are less than those in the F–L expansion by Cloude [2], [3]. That is to say, this inversion is better conditioned, and the system is less sensitive to errors for single- and dual-baseline data.

Moreover, we apply it to a real scenario using Chinese airborne X-band POLinSAR single-baseline data. The Chinese POLinSAR flight took place on January 8, 2010. They are the first dual-antenna polarimetric data in China. The instrument developed by East China Research Institute of Electronic Engineering, China Electronics Technology Group Corporation, collected quad-polarization images at X-band. The incidence angle was about 50°. The resolution of a pixel is 1 m.

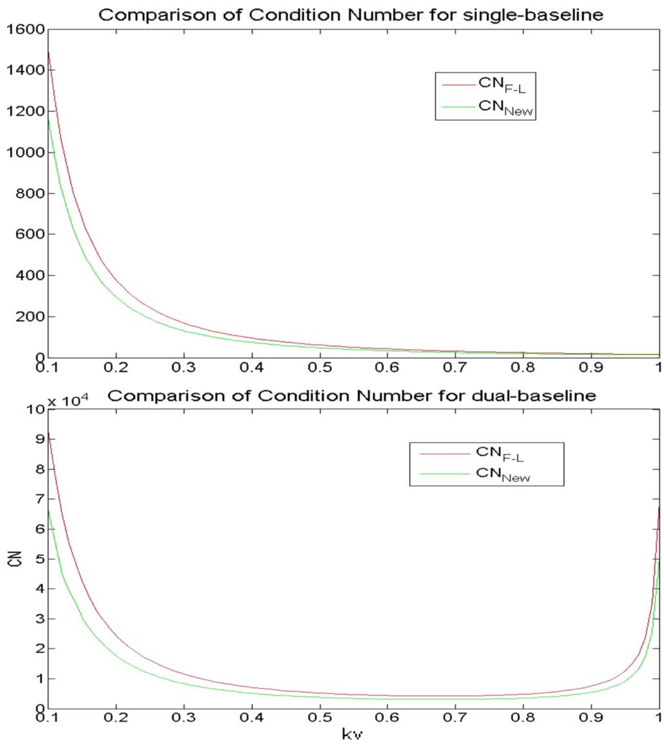

Fig. 5. Variations of CN with two expansions. (Top) Single baseline and (bottom) dual baseline (the k_v of the second baseline is one; the k_v of the first baseline changes between [0, 1]).

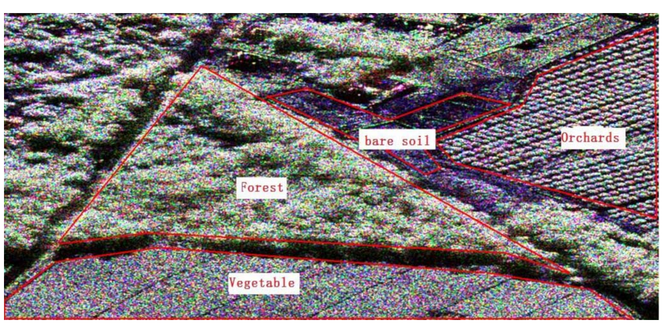

Fig. 6. High-resolution X-band POLinSAR data. RGB representation of the Pauli basis (HH + VV HV HH − VV).

The test site is located in Lingshui Li Minority Autonomous County with a geographical position at $18°22'$–$18°47'$ north and $109°45'$–$110°08'$ east, Hainan province, China. In our test site, the forest is mainly temperate and broad-leaved, and the forest height mainly ranges from 10 to 20 m. The test area which we choose is composed of orchards, bare fields, sparse forests, vegetable patches, and buildings. Moreover, the study area is flat; the reference tree height data are collected by ground test. The Pauli decomposition is shown in Fig. 6.

HH polarization channel is used to generate the estimation of the vertical structure of the forest in the F–L expansion and the new expansion, respectively, as shown in Fig. 7. Moreover, the calculated mean and variance of a_{10} in the F–L expansion are -0.92 and 0.72, respectively, while those of a_{10} in our method are -0.51 and 0.40, respectively. It is concluded that a_{10} in the new series exhibits less volatility, and therefore, the consequences possess better condition.

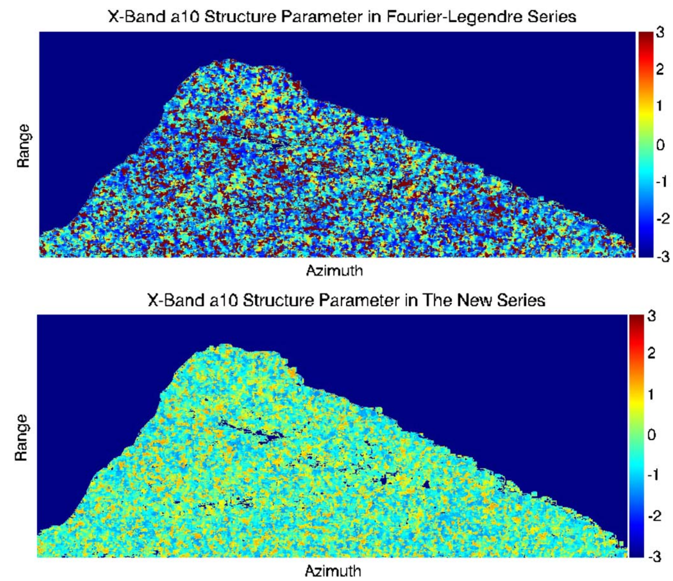

Fig. 7. Images of a_{10} in (top) the F–L expansion and (bottom) our new expansion.

V. Conclusion

In this letter, we have introduced a new function expansion for PCT and validated it using POLSARPro-simulated single-baseline and Chinese airborne X-band POLinSAR data.

In the F–L expansion proposed by Cloude, it provides two complex coherences on the dual-baseline case; four coefficients can be estimated, and the highest polynomial order used to approximate is four. In the new expansion, the highest order is six, and the results can exhibit the internal fine structure. In addition, due to better conditioning of the matrix inversion, the profile coefficients are less susceptible to noise, which is always present in SAR interference processing.

Further analysis is to be required to investigate multibaseline applications in the new expansion. Moreover, we do not take the effects of the number of looks and the frequency change into account, which both affect the final results.

Acknowledgment

The authors would like to thank the anonymous referees for their useful suggestions for improving the clarity of this letter.

References

[1] K. P. Papathanassiou and S. R. Cloude, "Single baseline polarimetric SAR interferometry," *IEEE Trans. Geosci. Remote Sens.*, vol. 39, no. 11, pp. 2352–2363, Nov. 2001.

[2] S. R. Cloude, "Polarization coherence tomography," *Radio Sci.*, vol. 41, no. 1, p. RS4017, Aug. 2006.

[3] S. R. Cloude, "Dual-baseline coherence tomography," *IEEE Trans. Geosci. Remote Sens. Lett.*, vol. 4, no. 1, pp. 127–131, Jan. 2007.

[4] S. R. Cloude, "Multibaseline polarization coherence tomography," presented at the 3rd Int. Workshop Science Applications SAR Polarimetry Polarimetric Interferometry (POLINSAR), Frascati, Italy, Jan. 22–27, 2007, ESRIN, Paper ESA SP-586, ESRIN.

[5] S. R. Cloude and K. P. Papathanassiou, "Three-stage inversion process for polarimetric SAR interferometry," *Proc. Inst. Elect. Eng.—Radar Sonar Navig.*, vol. 150, no. 3, pp. 125–134, Jun. 2003.